Macromolecular Rapid Communications
www.mrc-journal.de

Intrinsically Microporous Polymer Nanosheets for High-Performance Gas Separation Membranes

*Marzieh Tamaddondar, Andrew B. Foster, Jose M. Luque-Alled, Kadhum J. Msayib, Mariolino Carta, Sara Sorribas, Patricia Gorgojo, Neil B. McKeown, and Peter M. Budd**

Microporous polymer nanosheets with thicknesses in the range 3–5 nm and with high apparent surface area (Brunauer–Emmett–Teller surface area 940 $m^2 g^{-1}$) are formed when the effectively bifunctional (tetrafluoro) monomer used in the preparation of the prototypical polymer of intrinsic microporosity PIM-1 is replaced with an effectively tetrafunctional (octafluoro) monomer to give a tightly crosslinked network structure. When employed as a filler in mixed-matrix membranes based on PIM-1, a low loading of 0.5 wt% network-PIM-1 nanosheets gives rise to enhanced CO_2 permeability and CO_2/CH_4 selectivity, compared to pure PIM-1.

Membrane technology offers the prospect of straightforward and energy-efficient gas separation processes.[1] Membranes are needed that exhibit good selectivity in combination with high permeability. Robeson[2] established the upper bounds of performance that could be achieved for industrially important gas pairs with the polymeric membranes available in 1991. A class of high free volume, glassy polymers introduced in 2004, referred to as polymers of intrinsic microporosity (PIMs),[3] contributed to a revision in 2008 of the upper bounds,[4] and a further revision in 2015 for some gas pairs.[5] Recently, the upper bounds for CO_2/CH_4 and CO_2/N_2 were redefined[6] on the basis of data for some new PIMs. The quest for high-performance gas separation membranes has extended to the use of 2D materials,[7,8] such as graphene[9] and graphene oxide,[10] inorganic nanosheets including zeolites,[11] transition metal dichalcogenides[12] and MXenes,[13] metal–organic framework nanosheets,[14] and covalent organic framework nanosheets.[15,16] Membrane properties may be tailored by combining 2D materials or other fillers with processable polymers to form mixed matrix membranes (MMMs).[17]

Recently, attention has turned to the formation of porous organic polymeric nanosheets through polymerization.[18] Here, we introduce a new type of nanosheet created as a highly crosslinked analogue of a linear PIM. The tetrafluoro-monomer utilized in the synthesis of the prototypical polymer of intrinsic microporosity, PIM-1 (**Figure 1**a), was replaced with an octafluoro-monomer to form a tightly linked network polymer, network-PIM-1 (Figure 1b). The gas permeation behavior was investigated for MMMs of network-PIM-1 with PIM-1 itself. The original concept was to create highly compatible fillers for use in MMMs. Surprisingly, pronounced effects were observed at very low filler concentrations, analogous to the effects seen with 2D materials such as graphene.[19] Further studies revealed that the polymerization gave rise to a nanosheet morphology, as discussed below.

Network-PIM-1 was synthesized following the original procedure for PIM-1 synthesis,[20] replacing the tetrafluoro-monomer (tetrafluoroterephthalonitrile) with an octafluoro-monomer (4,4′-dicyano-2,2′,3,3′,5,5′,6,6′-octafluorobiphenyl) in the appropriate stoichiometric ratio. The product was insoluble in all common solvents.

Elemental analysis of a fully reacted, ideal network-PIM-1 structure, $C_{56}H_{40}N_2O_8$, would be expected to give: C, 77.40, H, 4.65; N, 3.22 wt%. Experimental values for dried network-PIM-1 powder were: C, 71.04; H, 4.64; N, 3.38; F, 2.25 wt%. The residual fluorine shows that some of the biphenyl units from the octafluoro-monomer are not fully reacted. This is unsurprising in a kinetically controlled step-growth polymerization, given the steric hindrance at a site with such a high density of functional groups.

The C/N ratio from elemental analysis can provide an insight into the relative proportions of spiro and biphenyl units incorporated into the network-PIM-1 structure. For complete reaction of two spiro units for each biphenyl unit, the expected C/N weight ratio is 24.01. The experimental C/N weight ratio of 21.02 is consistent with a structure having

Dr. M. Tamaddondar, Dr. A. B. Foster, Dr. S. Sorribas, Prof. P. M. Budd
Department of Chemistry
University of Manchester
Manchester, M13 9PL, UK
E-mail: Peter.Budd@manchester.ac.uk
J. M. Luque-Alled, Dr. P. Gorgojo
Department of Chemical Engineering and Analytical Science
University of Manchester
Manchester, M13 9PL, UK
Dr. K. J. Msayib, Prof. N. B. McKeown
EastChem
School of Chemistry
University of Edinburgh
David Brewster Road, Edinburgh, EH9 3FJ, UK
Dr. M. Carta
Department of Chemistry
College of Science
Swansea University
Grove Building, Singleton Park, Swansea, SA2 8PP, UK
The ORCID identification number(s) for the author(s) of this article can be found under https://doi.org/10.1002/marc.201900572.

DOI: 10.1002/marc.201900572

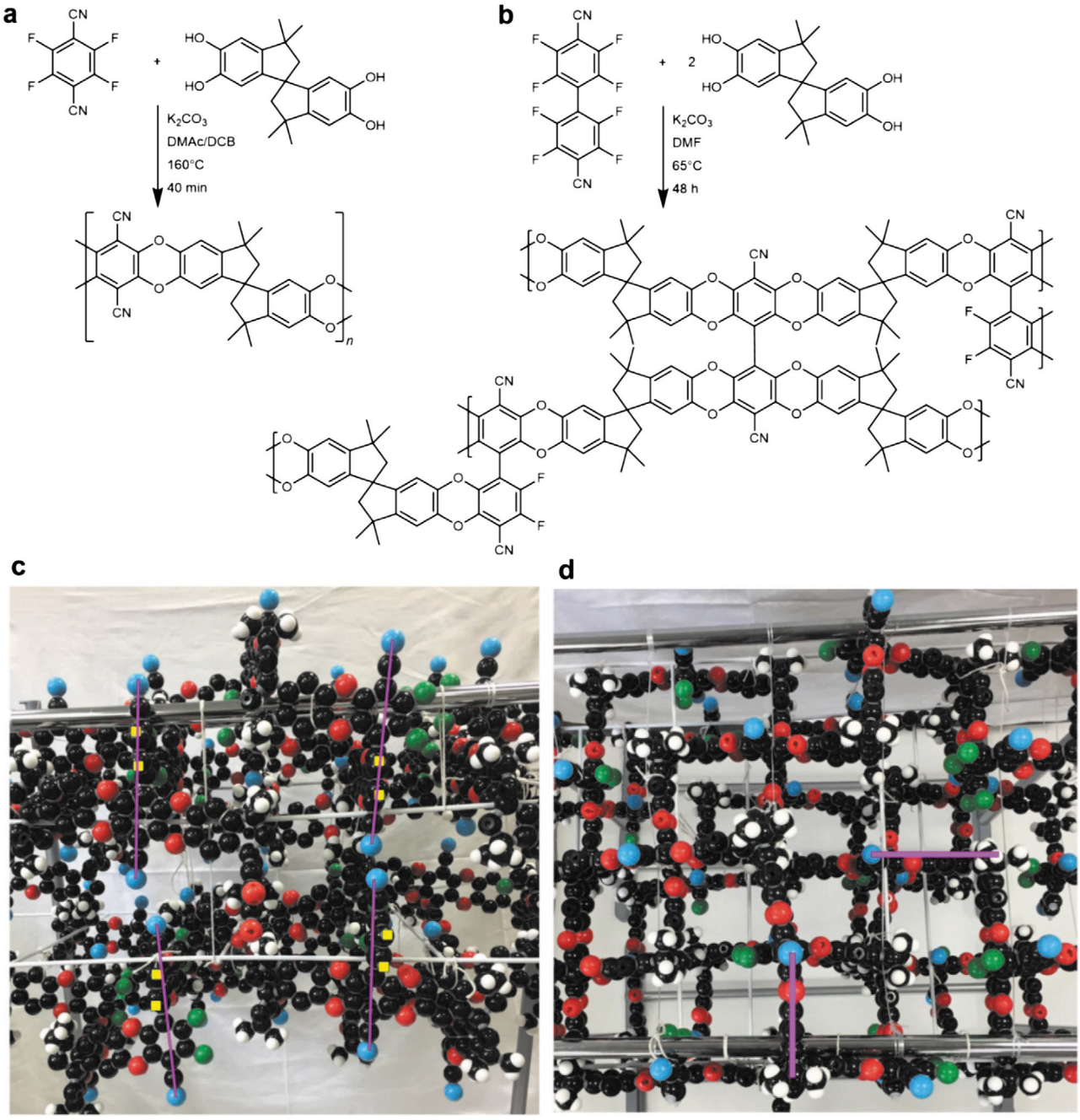

Figure 1. Polymer preparation. a) PIM-1 synthesis in a mixed solvent of dimethylacetamide (DMAc) and dichlorobenzene (DCB). b) Network-PIM-1 synthesis in dimethylformamide (DMF), showing a feasible fragment of the network structure based on elemental analysis. c) Side view of model of network-PIM-1 nanosheet structure; mauve lines indicate the length of a biphenyl unit (1.2 nm); yellow squares indicate positions where further reaction with a spiro monomer unit is possible. d) Top view of model of network-PIM-1 nanosheet structure; mauve lines indicate distance from center of biphenyl unit to midpoint of an attached spiro unit (0.8 nm); green atoms are unreacted fluorine atoms where steric hindrance prevents further reaction.

about five spiro units for every three biphenyl units, as indicated in Figure 1b.

Solid-state ^{13}C NMR spectroscopy (Figure S5, Supporting Information) and Fourier transform infra-red spectroscopy (Figure S6, Supporting Information) of network-PIM-1 show essentially the same features as PIM-1 itself, confirming the chemical similarity of the two materials. The powder X-ray diffraction (PXRD) pattern (Figure S9, Supporting Information) of network-PIM-1 was similar to that of PIM-1, which shows three peaks at 2θ values corresponding to d spacings of 6.7, 5.2, and 3.9 Å, superimposed on a smooth shoulder.[21,22]

Images from atomic force microscopy (AFM) at two different resolutions are shown in **Figure 2**a,b for network-PIM-1 particles deposited onto a silicon wafer from an ultra-dilute

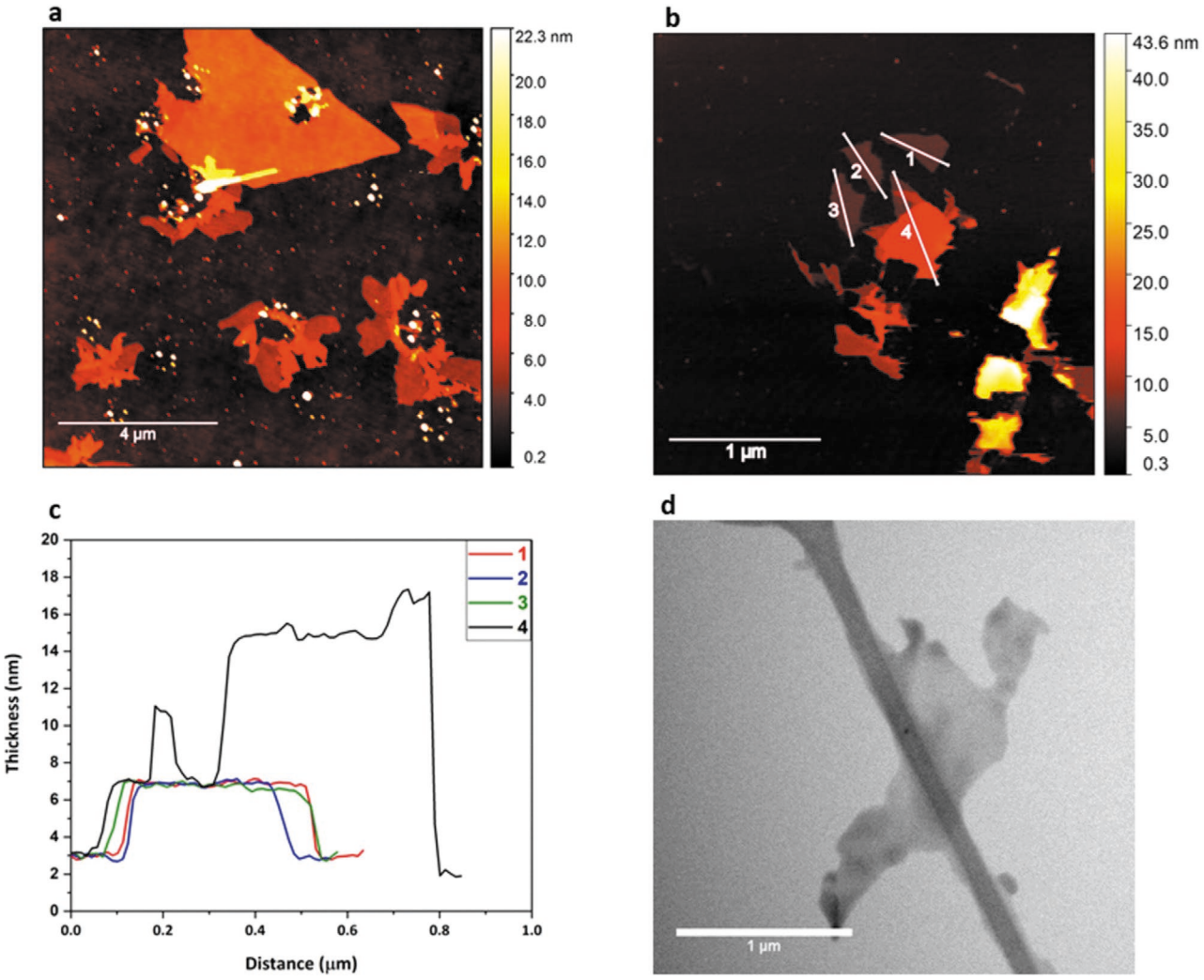

Figure 2. Characterization of network-PIM-1 nanosheets. a) AFM image of network-PIM-1 nanosheets. b) AFM image of network-PIM-1 nanosheets showing four lines for which height profiles were taken. c) Height profiles from AFM related to lines 1–4 in image (b). d) Bright field STEM image of network-PIM-1 nanosheet.

dispersion in chloroform. Extended sheet-like structures are seen, with lateral sizes ranging from a few hundred nanometers to a few micrometers. The height profiles associated with some of the structures (represented by lines 1–4 in Figure 2b) are shown in Figure 2c. The thickness versus distance plots of lines 1–3, which may be attributed to single sheets of network-PIM-1, show thicknesses in the range 3–5 nm and lateral sizes of a few hundred nanometers. The height profile related to line 4 shows a jump in the thickness to around 15 nm, which may be related to the stacking of three or more layers. The AFM results suggest that network-PIM-1 is composed of nanosheets with a high aspect ratio (≈100) and thicknesses of a few nanometers.

Further evidence for a nanosheet morphology comes from transmission electron microscopy (TEM), operated in scanning transmission electron microscopy (STEM) mode, of network-PIM-1 deposited from chloroform onto a lacey carbon grid (Figure 2d). Elemental mapping for C, N, O, and F by energy dispersive X-ray spectroscopy (EDX) (Figure S8, Supporting Information) confirms the presence of organic sheet-like structures. It should be mentioned that Cu was also mapped during the EDX analysis, as it was one of the elements present in the substrate used for TEM/EDX. Additionally, a trace of K was detected in network-PIM-1, which might be due to a small quantity of potassium carbonate entrapped in the crosslinked structures during the polymerization. Scanning electron microscopy (SEM) images of network-PIM-1 are also presented in Figure S7, Supporting Information. These images suggest the presence of extended structures, which might be related to single or aggregated particles.

The question arises as to why network-PIM-1 has a nanosheet morphology. There is innate anisotropy in the monomers, so that reaction will give a structure in which there is a degree of orientational order, with the nitrile groups tending to point along the same axis. For linear PIM-1, the chain can bend and flex sufficiently that a preferred orientation is not maintained over its

entire length. However, for network-PIM-1 with a high crosslink density, the necessity for multiple connections at biphenyl units leads to a large number of small macrocycles that maintain the rigidity of the structure. A molecular model of a feasible fragment of nanosheet structure is shown in Figure 1c,d. The side view in Figure 1c illustrates the preferred orientation of the biphenyl units (some are marked by mauve lines) and shows, as yellow squares, sites where the structure can be extended in a transverse direction. The top view in Figure 1d shows that there are no sites for reaction on that face. Thus, as the structure is built up during step-growth polymerization, it is relatively easy to extend in directions perpendicular to that defined by the orientation of the nitrile groups, but there are few options for extending out of that plane. Computer simulation studies are in progress to obtain a fuller understanding of nanosheet formation.

Although network-PIM-1, like PIM-1 itself, is essentially amorphous, the model shown in Figure 1c,d indicates a high degree of orientational order within a layered structure, akin to a smectic liquid crystal, albeit locked into a network rather than fluid as in a liquid crystal. Such a structure is expected to exhibit birefringence. Polarized light microscopy (Figure S11, Supporting Information) of a membrane with 20 wt% network-PIM-1 filler, at which loading there is some agglomeration of filler particles, demonstrates that the filler particles are strongly birefringent, unlike the background of PIM-1 itself.

The N_2 adsorption/desorption isotherm at 77 K for network-PIM-1 is compared with that for a sample of conventional PIM-1 in **Figure 3**a. Both polymers show high uptake at low relative pressure, which is characteristic of a microporous material (pore size < 2 nm) as defined by IUPAC.[23] Network-PIM-1 shows slightly higher uptake of N_2 than PIM-1, reflected in a higher apparent surface area from Brunauer–Emmett–Teller (BET) analysis (940 ± 7 m^2 g^{-1} for network-PIM-1 compared with 780 ± 7 m^2 g^{-1} for PIM-1). CO_2 adsorption isotherms at 273 K (Figure 3b) similarly show higher uptake for network-PIM-1 than for PIM-1. This translates into a slight enhancement in CO_2 uptake when small amounts of network-PIM-1 are incorporated into a PIM-1 membrane (Figure 3c).

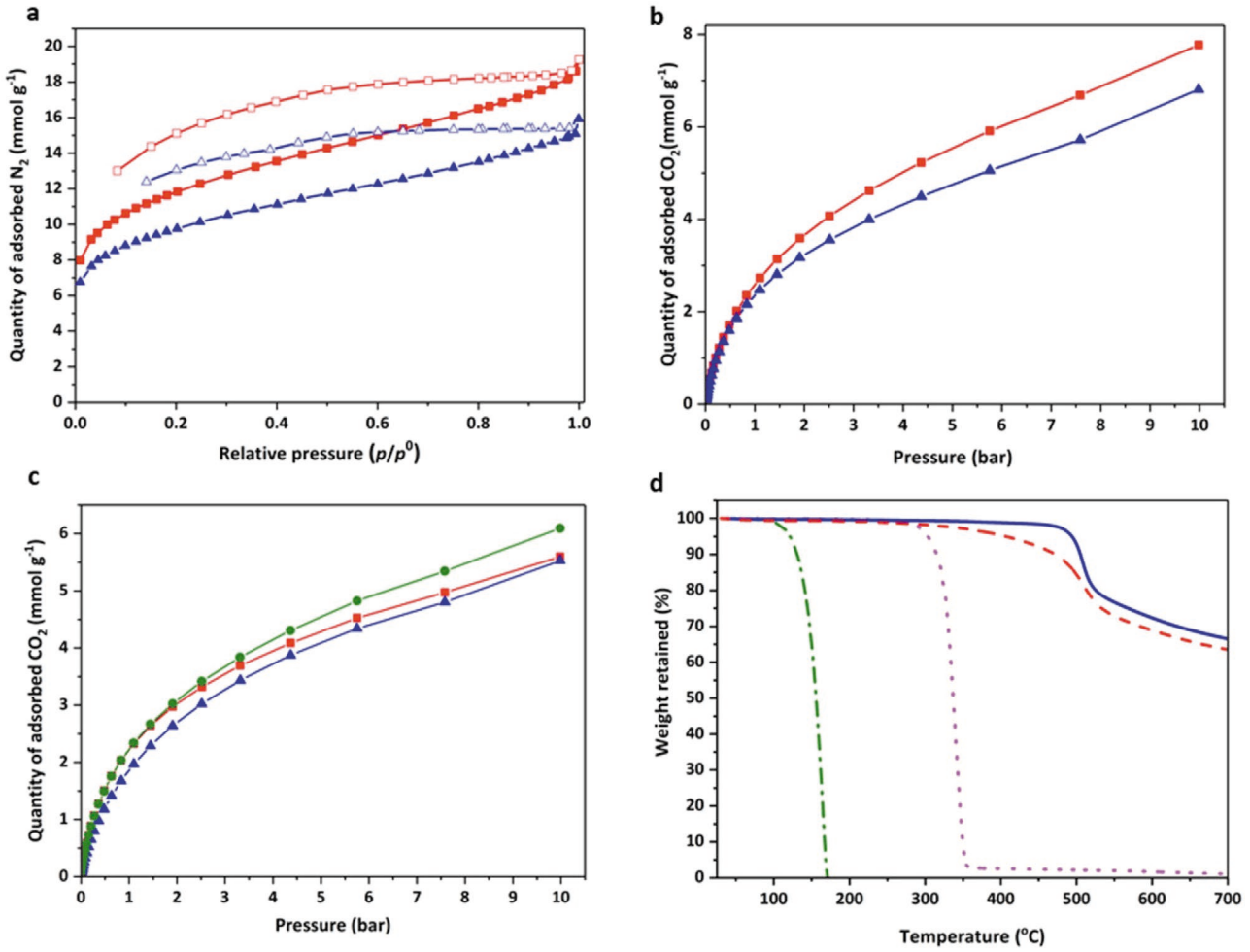

Figure 3. Gas sorption analysis and thermogravimetric analysis of network-PIM-1 and PIM-1. a) N_2 adsorption (filled symbols) and desorption (empty symbols) isotherms at 77 K for network-PIM-1 (■,□) and PIM-1 (▲,△) powders. b) CO_2 adsorption isotherms at 273 K for network-PIM-1 (■) and PIM-1 (▲) powders. c) CO_2 adsorption isotherms at 273 K for a PIM-1 membrane (▲) and for MMMs of network-PIM-1 in PIM-1 at filler loadings of 0.5 wt% (■) and 5 wt% (●), all methanol-treated. d) TGA analysis of network-PIM-1 (- - -) and PIM-1 (——) powders and of the octafluoro- (- — -) and spiro- (· · ·) monomers used to prepare network-PIM-1.

Thermogravimetric analysis (TGA) of network-PIM-1 is compared with that of PIM-1 in Figure 3d. Under the conditions of the experiment, PIM-1 does not show any significant weight loss below 450 °C. Network-PIM-1 shows a modest weight loss in the temperature range 330–450 °C, which may indicate that there are some labile short branches in the structure. The monomers used to prepare network-PIM-1 show weight losses at lower temperatures than the polymer, as can be seen in Figure 3d.

Self-standing MMMs were prepared for gas permeation measurements with 0.027, 0.2, 0.5, 5, and 10 wt%, with respect to the total solids content, of network-PIM-1 in PIM-1. Pure PIM-1 membranes were also prepared for comparison. Membrane thicknesses were in the range 59–80 µm. Attempts to prepare MMMs with higher network-PIM-1 loadings resulted in excessively brittle membranes, but a sample with 20 wt% loading was utilized for polarized light microscopy (Figure S11, Supporting Information). SEM images (Figure S10, Supporting Information) show evidence of filler agglomeration at loadings of 5 and 10 wt%. Despite the apparent chemical similarity of the network-PIM-1 and PIM-1 structures, there is a tendency to segregation at higher filler loadings, which may be attributed, at least in part, to the nanosheet structure of the network polymer.

Membranes were immersed in methanol for 15 h and then dried prior to carrying out measurements. This procedure opens up free volume in the membrane, helps to flush out residual solvents, and reverses the effects of membrane history.

Mixed gas CO_2/CH_4 (1:1, v/v) permeation data for methanol-treated membranes with network-PIM-1 loadings up to 10 wt% are shown in **Figure 4**a. Pure PIM-1 exhibited a CO_2 permeability of 5920 Barrer, within the range of values previously reported for PIM-1. This represents orders of magnitude higher permeability than is achieved for traditional membrane polymers.

At network-PIM-1 loadings of 0.2 and 0.5 wt%, there is an enhancement in gas permeabilities, the CO_2 permeability rising to 9780 Barrer for the 0.5 wt% MMM. Enhanced gas permeabilities at low filler loadings have previously been observed for MMMs of graphene in PIM-1,[19] which may be attributed, at least in part, to the effect of the sheet-like nanofiller on the packing of the PIM-1 polymer chains. At higher network-PIM-1 loadings, the permeabilities are in a similar range to PIM-1 alone, but with 10 wt% network-PIM-1 the CO_2/CH_4 selectivity is enhanced. Unlike graphene, network-PIM-1 is a porous material through which gas permeation can occur, but the highly crosslinked structure may modify the selectivity to different gases. Gas permeation can often be understood in terms of a solution-diffusion model, in which the permeating species first undergo sorption or dissolution in the membrane on the feed side, then diffuse through the membrane, and finally desorb on the permeate side. In this model, the permeability coefficient, P, can generally be expressed as the product of a sorption or solubility coefficient, S, and a diffusion coefficient, D (Equation (1)).

$$P = SD \tag{1}$$

For a binary system, selectivity is expressed as a ratio of permeabilities, and differences in selectivity may arise from differences in S and/or from differences in D. It was shown above that network-PIM-1 shows enhanced CO_2 sorption compared to PIM-1. The tightly linked structure is likely also to modify the diffusion coefficient.

It should be noted that most gas permeation studies in the literature are carried out with pure gases. Mixed gas permeation studies, as undertaken in the present work, are more realistic and can reveal permeation behavior different to that observed with pure gases, particularly for mixtures involving

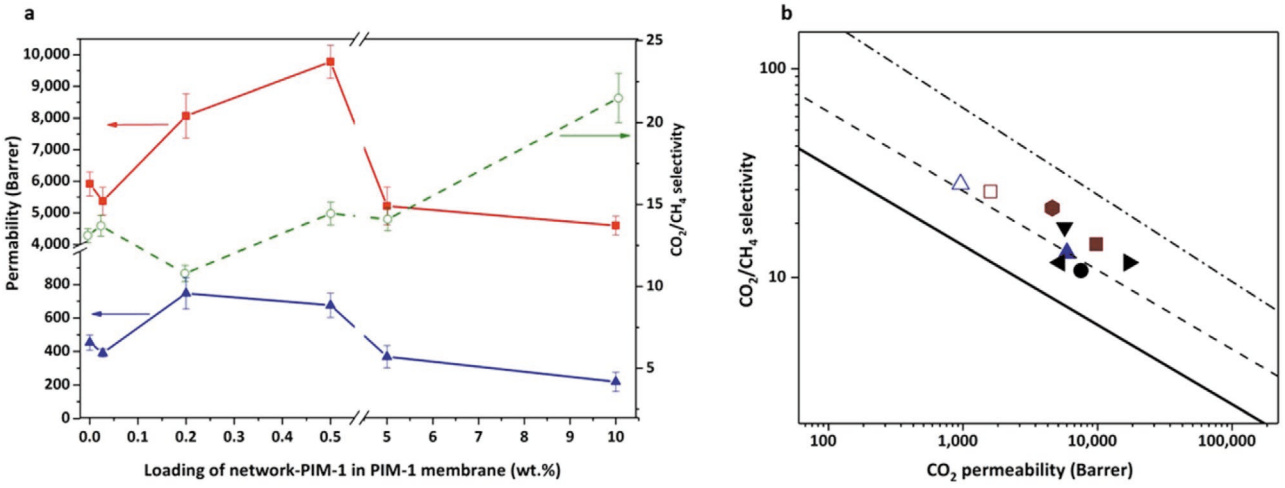

Figure 4. CO_2 and CH_4 permeation. a) CO_2 permeability (■), CH_4 permeability (▲), and CO_2/CH_4 selectivity (○) for methanol-treated membranes with various loadings of network-PIM-1 in PIM-1; measurements were carried out with a mixed gas CO_2/CH_4 (1:1, v/v) feed at a temperature of 25 °C and transmembrane pressure of 2 bar; each data point is an average for three membrane samples and the standard deviation is indicated by the error bars. b) Double logarithmic plot of CO_2/CH_4 selectivity against CO_2 permeability showing 1991 (——),[2] 2008 (- - -),[4] and 2019 (- · - ·)[6] upper bounds, with data from this work for PIM-1 (▲) and MMMs with 0.5 wt% (■) and 10 wt% (⬢) network-PIM-1 3 days after methanol treatment, and for PIM-1 (△) and the MMM with 0.5 wt% network-PIM-1 (□) after 7 months aging; also shown are data from the literature for MMMs of PIM-1 with 24.2 wt% ZIF-8 (▶),[27] 0.5 wt% f-MWCNT (●),[28] 2 wt% SNW-1 (◀),[29] and 0.126 wt% rGO-OA (▼).[30]

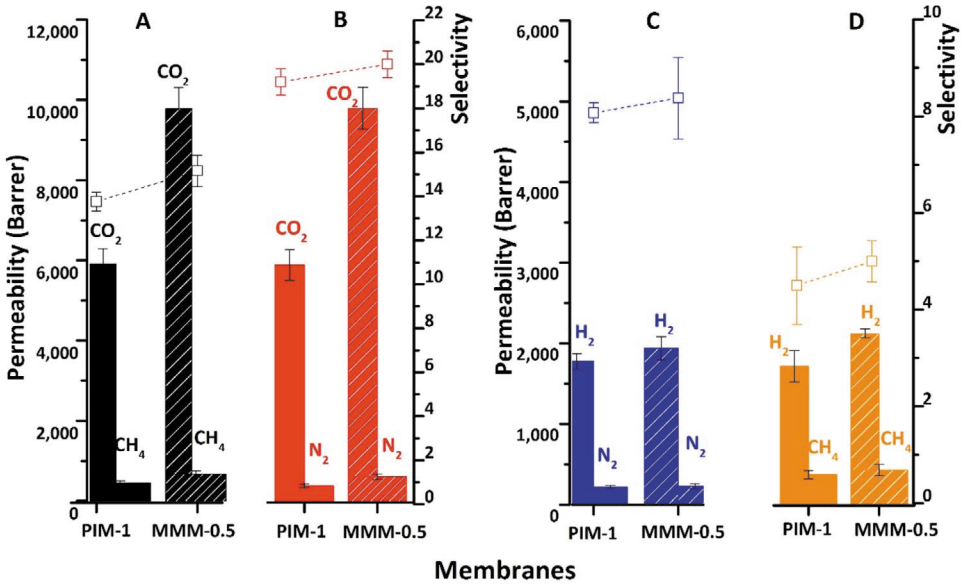

Figure 5. Gas permeabilities (columns, left axes) and selectivities (squares, right axes) for methanol-treated membranes with 0.5 wt% network-PIM-1 in PIM-1, compared to pure PIM-1, for the gas mixtures A) CO_2/CH_4, B) CO_2/N_2, C) H_2/N_2, and D) H_2/CH_4 (all 1:1, v/v); all measurements were carried out 3 days after methanol treatment at a temperature of 25 °C and transmembrane pressure of 2 bar. Each data point is an average for three membrane samples and the standard deviation is indicated by the error bars.

highly condensable gases such as CO_2. The sorption coefficient for one gas may be reduced because of competitive sorption by the other,[24] or the diffusion of one gas may be hindered because of a "blocking" effect of the other.[25] In addition, the presence of highly soluble gases such as CO_2 may enhance the mobility of the polymer chains and bring about swelling of the polymer matrix, an effect referred to as plasticization. Swaiden et al.[26] previously investigated the pure and mixed gas CO_2/CH_4 separation properties of PIM-1, and found that for CO_2 the mixed gas permeability was lower than the pure gas permeability (attributed to competition for CO_2 sorption sites by copermeating CH_4), while for CH_4 the mixed gas permeability was higher than the pure gas permeability (attributed to enhanced diffusion of CH_4 due to a plasticizing effect of CO_2). Both effects give rise to lower mixed gas CO_2/CH_4 selectivity than expected from pure gas measurements.

Gas permeation data for different membrane materials may conveniently be compared on double logarithmic Robeson[2,4] plots of selectivity, for a pair of gases, versus the permeability of the fastest gas. Figure 4b shows that MMMs with 0.5 wt% and 10 wt% network-PIM-1 exceed Robeson's 2008 upper bound[4] and move toward the recently proposed 2019 upper bound for the CO_2/CH_4 gas pair.[6] It is significant that a change in polymer topology from linear to network can have such a pronounced effect, and this is being explored further in ongoing research. For comparison, representative data from the literature are also shown for MMMs of PIM-1 with the zeolitic imidazolate framework ZIF-8,[27] functionalized multi-walled carbon nanotubes (f-MWCNT),[28] the covalent organic framework SNW-1,[29] and octyl-functionalized reduced graphene oxide (rGO-OA).[30]

High free volume, glassy polymers such as PIMs are nonequilibrium systems that tend to lose free volume, and hence permeability, over time, in a process referred to as physical aging.[31] Permeation data after 7 months aging are included in Figure 4b for PIM-1 and for the MMM with 0.5 wt% network-PIM-1. As expected, both systems show a loss of permeability over time, accompanied by an increase in selectivity. The small loading of network in the MMM does not suppress aging, but it maintains an enhanced permeability relative to PIM-1.

The performance of membranes with 0.5 wt% network-PIM-1 was checked for three further gas mixtures: CO_2/N_2, H_2/N_2, and H_2/CH_4 (all 1:1, v/v). Permeabilities and selectivities for all the gas mixtures are shown in **Figure 5**. The most pronounced effects were seen for the strongly sorbing gas CO_2. As mentioned above, CO_2 adsorption experiments show that addition of network-PIM-1 to a PIM-1 membrane leads to an enhancement of CO_2 sorption (Figure 3c).

This work demonstrates a new route to the formation of porous polymer nanosheets and introduces a new class of nanofiller with potential for use in high-performance mixed matrix membranes. Promising results are obtained for carbon dioxide separations.

Experimental Section

Synthesis of PIM-1: PIM-1 (M_w = 158 000 g mol^{-1}, M_w/M_n = 2.95) was synthesized by a variation of the high-temperature method proposed by Du et al.[32] and details are given in the Supporting Information.

Synthesis of Network-PIM-1: 4,4′-Dicyano-2,2′,3,3′,5,5′,6,6′-octafluorobiphenyl monomer was synthesized as reported by Taylor et al.[33] and details are given in the Supporting Information.

Well-dried 4,4′-dicyano-2,2′,3,3′,5,5′,6,6′-octafluorobiphenyl (0.483 g, 1.4 mmol), 5,5′,6,6′-tetrahydroxy-3,3,3′,3′-tetramethyl-1,1′-spirobisindane (TTSBI, 0.946 g, 2.8 mmol), and potassium carbonate (K_2CO_3, 3.073 g, 22.4 mmol) were added to a two-neck round bottom flask and the mixture was stirred under dry N_2 at room temperature for

30 min. Then, 20 mL of anhydrous DMF was added and the temperature was set at 65 °C. After 24 h, the reaction mixture was highly viscous and 12 mL more solvent was added to the system to avoid premature termination of the reaction. The reaction was continued for a total of 48 h and then stopped by quenching the reaction product in deionized water and some very dilute HCl. Then, the precipitate was filtered off and dried very well under reduced vacuum (3 h at room temperature). The crude polymer was washed with acetone (200 mL) and methanol (200 mL), after which it was filtered and dried again under vacuum at room temperature. The reaction product then underwent overnight-reflux with different solvents in a sequence of DMF (400 mL, 163 °C), THF (400 mL, 77 °C), chloroform (400 mL, 71 °C), acetone (400 mL, 66 °C), and two times methanol (400 mL, 74 °C). After each time refluxing with a solvent, the product was filtered while still hot, re-washed with fresh hot solvent, and then dried well under suction at room temperature for 2 h. The polymeric sample was washed with the next solvent before being refluxed again. Finally, the polymer was dried overnight under reduced pressure at 130 °C to give 0.89 g of network-PIM-1 (yield 73%). Full characterization results are provided in the Supporting Information.

Characterization Methods: For PIM-1, weight-average molecular weight (M_w), number-average molecular weight (M_n), and polydispersity index (M_w/M_n) were measured using multi-detector gel permeation chromatography (Viscotek GPCmax VE2001 solvent/sample module with TDA302 triple detector array), with two Polymer Lab mixed bead columns (PL Mixed B ×2). Measurements were performed using filtered chloroform as the eluent at a flow rate of 1 mL min^{-1}.

^1H and ^{13}C NMR spectra were collected with a Bruker DPX 400 MHz spectrometer at room temperature. Solid-state ^{13}C cross-polarization/magic angle spinning (CP-MAS) NMR was conducted at room temperature using a Bruker AVANCE III 400 MHz instrument with a static wide line probe (Bruker, 40–163 MHz).

Infrared spectra of solids were recorded on a Thermoscientific Nicolet iS5, iD5 spectrometer annexed to a Whatman FTIR purge gas generator. The spectra were recorded in the attenuated total reflectance (ATR) mode, with a resolution of 0.25 cm^{-1}, a sensitivity of 1, and 16 scans in the range 4000–500 cm^{-1}.

STEM and EDX data were obtained using a FEI Tecnai G2 20 equipped with an X-Max EDX detector. The TEM specimen was prepared by drop casting onto a lacey carbon grid of the solution in chloroform.

Tapping mode AFM (Bruker Multimode) was used to analyze the size and thickness of network-PIM-1 particles obtained from a drop of an ultra-dilute dispersion in chloroform cast on a silicon wafer substrate. 2D surface scanning images were computed automatically using Nanoscope Analysis software. The AFM 2D images were then analyzed by Gwyddion 2.50 software to obtain the height profile of the particles.

PXRD was performed using a Philips X' Pert Pro Diffractometer with Cu Kα radiation (1.54060 Å) generated by 20 mA current and 30 kV voltage. The PXRD patterns were collected at room temperature with 2θ value ranging from 3° to 50°, at a scanning rate of 20.95 s per step and a step size of 0.016°. The intersegmental spacing between polymer chains (d-spacing) was estimated by Bragg's law ($d = n\lambda/2\sin\theta$).

Polarized light microscopy images were obtained using a Leica DM 2500M Materials Analysis Microscope. A sample of MMM with 20 wt% network PIM-1 was mounted on a clean glass slide and the images were obtained at room temperature and 10× magnification.

A Micrometrics ASAP 2020 sorption analyzer was used to obtain N_2 adsorption/desorption isotherms at 77 K and to measure the BET surface areas. Samples were accurately weighed and about 0.10 g of the polymer was degassed at 120 °C for 16 h under high vacuum (10^{-5} bar) before starting the analysis. After cooling, degassed samples were reweighed, and placed in the analysis port. Nitrogen adsorption/desorption isotherms were undertaken at 77 K. Free space measurements were done after the sorption analysis and the obtained value was then used to correct the isotherms and the BET surface area.

CO_2 adsorption up to 10 bar at 273 K was conducted using a Micromeritics ASAP 2050 sorption analyzer. After degassing the samples (≈100 mg) at 120 °C for 16 h, the dried samples were transferred to the analysis port where CO_2 was injected to the sample and the amount of adsorbed CO_2 from 0 to 9 bar was measured.

TGA was used to establish the thermal degradation of the monomers and the two polymers. A Perkin-Elmer TGA System was used and the samples were heated to 1000 °C at a rate of 10 °C min^{-1} under nitrogen atmosphere.

Membrane Preparation: MMMs were prepared with different loadings of network-PIM-1 in PIM-1. As an example, the procedure for the fabrication of an MMM containing 5 wt% of network-PIM-1 is as follows:

PIM-1 (0.3 g) was dissolved in anhydrous chloroform (5 mL) by stirring the solution at room temperature for 12 h. A dispersion of network-PIM-1 (0.0159 g) in chloroform (5 mL) was prepared by stirring the mixture for 12 h at room temperature, followed by 10 min of sonication using a probe sonicator (Cole-Parmer Instruments, CPX 750, 750 watts). The PIM-1 solution was then added to the filler dispersion and the mixture was stirred magnetically for 1 day, followed by 10 min sonication. During the sonication, the mixture was kept in an ice bath and the sonication was done at intervals of 10 s to minimize the evaporation of the solvent. The homogenous mixture was then poured into an 8 cm diameter petri dish, which was covered and placed in a nitrogen cabinet for 48–72 h to allow for slow solvent evaporation. The formed membrane was then kept in a desiccator at room temperature for 2 days, followed by drying in a vacuum oven at 100 °C overnight to remove the remaining solvent.

Pure PIM-1 membranes were similarly prepared by casting a solution of PIM-1 (0.3 g) in anhydrous chloroform (10 mL).

Membranes were methanol-treated as follows:

The films were slowly immersed in a glass petri dish filled with methanol and were kept there for 15 h, during which the methanol was refreshed two times. Then, the films were removed and kept in a desiccator for 2 days at room temperature, then dried in a vacuum oven at 100 °C overnight.

Mixed Gas Permeation Measurements: Mixed gas permeability measurements were carried out as follows:

A binary feed mixture (25 mL min^{-1} of each gas) was used in a permeation apparatus employing the standard variable volume method. The total feed side pressure was set to ≈3 bar at T = 25 °C and the permeate side was at atmospheric pressure. Alicat Scientific mass flow controllers with the operating flow range of 0–100 ccm (cubic centimeter per minute) were used for the preparation of binary mixtures. Flat sheet membranes were masked between two aluminum-tape donuts and the membrane-aluminum interface was sealed using two-part potting epoxy (Araldite Rapid, Industrial MTCE Suppliers). Samples of 1 in. diameter were placed in the stainless steel permeation cell, where the two parts of the cell were sealed with rubber O-rings. Helium (60 mL min^{-1}) and Argon (10 mL min^{-1} or 60 mL min^{-1}) were used as the sweep gases for the analysis of permeates containing CO_2 and H_2, respectively. The sweep gas was at atmospheric pressure and was used to dilute the permeate gases and direct them to a micro gas chromatograph (GC, Agilent technologies 490) for automated on-line analysis of the permeate composition. The GC had two columns, MolSieve 5A and PoraPLOT U (PPU), with thermal conductivity detectors (TCD). PPU column was used for the analysis of CO_2 containing mixtures and MolSieve 5A was used for the analysis of H_2 containing mixtures. After measuring the flux of each gas, the permeability of the membranes was calculated using Equation (2)

$$P_i = \frac{N_i l}{(p_{i,1} - p_{i,2})} \tag{2}$$

where P_i is the permeability coefficient for component i in Barrer (1 Barrer = 10^{-10} cm^3 [STP] cm cm^{-2} s^{-1} $cmHg^{-1}$ = 3.35×10^{-16} mol m m^{-2} s^{-1} Pa^{-1}), N_i is the steady-state flux of penetrant i (cm^3 cm^{-2} s^{-1}), l is the membrane thickness (cm), and $p_{i,1}$ and $p_{i,2}$ are the partial pressures of component i in the feed (1) and permeate (2) side (in cm Hg). The selectivity was calculated as the ratio of the permeabilities for a pair of gases. The stage cut, the ratio of the flow rate of permeated gases (CO_2 and CH_4) to the flow rate in the feed, was less than 0.01 in all experiments.

Supporting Information

Supporting Information is available from the Wiley Online Library or from the author.

Acknowledgements

The authors gratefully acknowledge funding from the Engineering and Physical Sciences Research Council (EPSRC) Programme Grant EP/M01486X/1 "From membrane material synthesis to fabrication and function (SynFabFun)". All research data supporting this publication are directly available within this publication and the supporting information.

Conflict of Interest

The authors declare no conflict of interest.

Author Contributions

N.B.M., P.M.B., and P.G. designed the study; K.J.M. and M.C. carried out the initial work on the synthesis of network-PIM-1, which was continued by M.T.; S.S., A.B.F., and J.M.L.-A. contributed to characterization of the membranes and gas permeation studies. The manuscript was drafted by M.T. and all authors participated in the editing of the manuscript.

Keywords

crosslinking, gas separation, mixed matrix membranes, nanosheets, network-PIM-1, polymers of intrinsic microporosity

Received: October 28, 2019
Revised: November 22, 2019
Published online: December 17, 2019

[1] H. B. Park, J. Kamcev, L. M. Robeson, M. Elimelech, B. D. Freeman, *Science* **2017**, *356*, 1137.
[2] L. M. Robeson, *J. Membr. Sci.* **1991**, *62*, 165.
[3] P. M. Budd, B. S. Ghanem, S. Makhseed, N. B. McKeown, K. J. Msayib, C. E. Tattershall, *Chem. Commun.* **2004**, 230.
[4] L. M. Robeson, *J. Membr. Sci.* **2008**, *320*, 390.
[5] R. Swaidan, B. Ghanem, I. Pinnau, *ACS Macro Lett.* **2015**, *4*, 947.
[6] B. Comesaña-Gándara, J. Chen, C. G. Bezzu, M. Carta, I. Rose, M.-C. Ferrari, E. Esposito, A. Fuoco, J. C. Jansen, N. B. McKeown, *Energy Environ. Sci.* **2019**, *12*, 2733.
[7] G. Liu, W. Jin, N. Xu, *Angew. Chem., Int. Ed.* **2016**, *55*, 13384.
[8] M. Liu, P. A. Gurr, Q. Fu, P. A. Webley, G. G. Qiao, *J. Mater. Chem. A* **2018**, *6*, 23169.
[9] M. S. H. Boutilier, D. Jang, J.-C. Idrobo, P. R. Kidambi, N. G. Hadjiconstantinou, R. Karnik, *ACS Nano* **2017**, *11*, 5726.
[10] D. Bouša, K. Friess, K. Pilnáček, O. Vopička, M. Lanč, K. Fónod, M. Pumera, D. Sedmidubský, J. Luxa, Z. Sofer, *Chem. - Eur. J.* **2017**, *23*, 11416.
[11] M. Y. Jeon, D. Kim, P. Kumar, P. S. Lee, N. Rangnekar, P. Bai, M. Shete, B. Elyassi, H. S. Lee, K. Narasimharao, S. N. Basahel, S. Al-Thabaiti, W. Xu, H. J. Cho, E. O. Fetisov, R. Thyagarajan, R. F. DeJaco, W. Fan, K. A. Mkhoyan, J. I. Siepmann, M. Tsapatsis, *Nature* **2017**, *543*, 690.
[12] D. Wang, Z. Wang, L. Wang, L. Hu, J. Jin, *Nanoscale* **2015**, *7*, 17649.
[13] L. Ding, Y. Wei, L. Li, T. Zhang, H. Wang, J. Xue, L.-X. Ding, S. Wang, J. Caro, Y. Gogotsi, *Nat. Commun.* **2018**, *9*, 155.
[14] Y. Peng, Y. Li, Y. Ban, W. Yang, *Angew. Chem., Int. Ed.* **2017**, *56*, 9757.
[15] H. Fan, A. Mundstock, A. Feldhoff, A. Knebel, J. Gu, H. Meng, J. Caro, *J. Am. Chem. Soc.* **2018**, *140*, 10094.
[16] S. Yuan, X. Li, J. Zhu, G. Zhang, P. Van Puyvelde, B. Van der Bruggen, *Chem. Soc. Rev.* **2019**, *48*, 2665.
[17] Y. Wang, X. Wang, J. Guan, L. Yang, Y. Ren, N. Nasir, H. Wu, Z. Chen, Z. Jiang, *Ind. Eng. Chem. Res.* **2019**, *58*, 7706.
[18] J.-J. Chen, T.-L. Zhai, Y.-F. Chen, S. Geng, C. Yu, J.-M. Liu, L. Wang, B. Tan, C. Zhang, *Polym. Chem.* **2017**, *8*, 5533.
[19] K. Althumayri, W. J. Harrison, Y. Shin, J. Gardiner, C. Casiraghi, P. M. Budd, P. Bernardo, G. Clarizia, J. C. Jansen, *Philos. Trans. R. Soc., A* **2016**, *374*, 20150031.
[20] P. M. Budd, E. S. Elabas, B. S. Ghanem, S. Makhseed, N. B. McKeown, K. J. Msayib, C. E. Tattershall, D. Wang, *Adv. Mater.* **2004**, *16*, 456.
[21] A. G. McDermott, G. S. Larsen, P. M. Budd, C. M. Colina, J. Runt, *Macromolecules* **2011**, *44*, 14.
[22] L. Hao, K.-S. Liao, T.-S. Chung, *J. Mater. Chem. A* **2015**, *3*, 17273.
[23] M. Thommes, K. Kaneko, A. V. Neimark, J. P. Olivier, F. Rodriguez-Reinoso, J. Rouquerol, K. S. W. Sing, *Pure Appl. Chem.* **2015**, *87*, 1051.
[24] N. Alaslai, B. Ghanem, F. Alghunaimi, E. Litwiller, I. Pinnau, *J. Membr. Sci.* **2016**, *505*, 100.
[25] M. Galizia, W. S. Chi, Z. P. Smith, T. C. Merkel, R. W. Baker, B. D. Freeman, *Macromolecules* **2017**, *50*, 7809.
[26] R. Swaidan, B. S. Ghanem, E. Litwiller, I. Pinnau, *J. Membr. Sci.* **2014**, *457*, 95.
[27] A. F. Bushell, M. P. Attfield, C. R. Mason, P. M. Budd, Y. Yampolskii, L. Starannikova, A. Rebrov, F. Bazzarelli, P. Bernardo, J. Carolus Jansen, M. Lanč, K. Friess, V. Shantarovich, V. Gustov, V. Isaeva, *J. Membr. Sci.* **2013**, *427*, 48.
[28] M. M. Khan, V. Filiz, G. Bengtson, S. Shishatskiy, M. M. Rahman, J. Lillepaerg, V. Abetz, *J. Membr. Sci.* **2013**, *436*, 109.
[29] X. Wu, Z. Tian, S. Wang, D. Peng, L. Yang, Y. Wu, Q. Xin, H. Wu, Z. Jiang, *J. Membr. Sci.* **2017**, *528*, 273.
[30] M. Alberto, R. Bhavsar, J. M. Luque-Alled, A. Vijayaraghavan, P. M. Budd, P. Gorgojo, *J. Membr. Sci.* **2018**, *563*, 513.
[31] Z.-X. Low, P. M. Budd, N. B. McKeown, D. A. Patterson, *Chem. Rev.* **2018**, *118*, 5871.
[32] N. Du, J. Song, G. P. Robertson, I. Pinnau, M. D. Guiver, *Macromol. Rapid Commun.* **2008**, *29*, 783.
[33] R. G. D. Taylor, C. G. Bezzu, M. Carta, K. J. Msayib, J. Walker, R. Short, B. M. Kariuki, N. B. McKeown, *Chem. - Eur. J.* **2016**, *22*, 2466.